Molecular treatment of electron capture in collisions of O^{5+} ions with H atoms at energies from 6 eV/amu to 10 keV/amu: Transfer-excitation processes

N. Shimakura
General Education Department, Niigata University, Niigata 950-21, Japan

S. Suzuki
Department of Chemistry, Faculty of Science, Niigata University, Niigata 950-21, Japan

M. Kimura
Argonne National Laboratory, Argonne, Illinois 60439
and Department of Physics, Rice University, Houston, Texas 77251

(Received 14 May 1993)

Electron capture in collisions of O^{5+} ions with H atoms is investigated theoretically by using a semiclassical molecular-orbital method in the energy range from 6 eV/amu to 10 keV/amu. Electron translation effects are properly included (to the first order of relative velocity). The primary contributors to electron capture are $O^{4+}(2s4l)$ states. However, two-electron transfer-excitation processes are also important in the entire energy range studied. The contribution from these processes amounts to 50% of the total at 1 keV/amu; it remains at 27% even at studied energy as low as 6 eV/amu. The $O^{4+}(2p3p\ ^3S)$ and $O^{4+}(2p3d\ ^3P)$ states for the triplet and the $O^{4+}(2p3p\ ^1S)$ state for the singlet contribute dominantly to the transfer-excitation process at low collision energies. Results of an analysis based on polarization parameters for electron capture are reported.

PACS number(s): 34.10.+x, 34.20.−b, 34.70.+e

I. INTRODUCTION

We have conducted a detailed study of electron-capture processes in collisions of multiply charged ions with H atoms for N^{5+} [1], N^{4+} [2], C^{5+} [3], and B^{4+} [4] projectiles over a wide range of collision energies by using a molecular-orbital-expansion method. In the previous studies, we provided sets of accurate cross sections essential for modeling and identified important dynamics of electron capture, an effect of polarization potential at low energy, and the origins of various structures seen in capture cross sections. In addition, we examined the role of two-electron processes (transfer excitation) that compete with normal capture in the dynamics of N^{4+} impact.

In this paper, we report the study of electron capture in collisions of O^{5+} ions with H atoms at collision energies from 6 eV/amu to 10 keV/amu. In the system, several two-electron transfer-excitation channels are observed near the initial ($O^{5+}+H$) channel, along with a band of single-capture channels. Hence, the transfer-excitation channels are expected to play a crucial role in electron capture. Furthermore, studies of the (l,m) distributions for the electron capture processes provide insight for understanding dynamic electron correlation effects.

Total cross sections of the electron capture processes for the ($O^{5+}+H$) system were first measured by Phaneuf *et al.* [5] with a time-of-flight method. This measurement and recent experiments by Havener *et al.* [6,7] using a merged-beam method combine to cover a wide range of energy from 0.1 eV/amu to 1 keV/amu and serve as a stringent test of theory. There have also been theoretical studies using a quantum-mechanical close-coupling method reported by Garguad [8] and more recently Andersson *et al.* [9] below 1 keV/amu. These authors employed a one-electron model and hence included only single-electron processes. Although their results appear to be in reasonable accord with the measurements, our calculation shows that the transfer-excitation process plays an essential role in the determination of capture dynamics and the neglect of these channels could cause gross errors in evaluation of the cross section except at the low-collision-energy limit. In connection with the present study, Macek and Ovchinnikov [10] recently evaluated the effect of the H atom in high Rydberg states on capture in O^{5+} + H collisions.

II. SUMMARY OF THEORETICAL TREATMENT

Details of the theory used have been provided elsewhere [11,12] and only a summary of theoretical framework is furnished here. However, full information on all of the parameters used in the calculation is given.

A. Molecular states

The molecular electronic states are obtained by using a valence-bond configuration-interaction method modified to include a Gaussian-type pseudopotential. The pseudopotential to represent the O^{6+} core has the form

$$V(\mathbf{r})=\sum_{l,m} V_l(r)|Y_{lm}\rangle\langle Y_{lm}| \quad (1)$$

and

TABLE I. O^{6+} pseudopotential parameters.

Parameter	Value (a.u.)
A_0	74.061 510 747 5
A_1	−3.393 394 430 87
A_2	−0.566 147 742 355
ξ_0	12.977 981 847 3
ξ_1	15.165 862 608 6
ξ_2	8.917 450 937 80
d	0.197 370 2
α_d	0.002 64
α_q	0.000 162

$$V_l(r)=A_l\exp(-\xi_l r^2)-\frac{\alpha_d}{2(r^2+d^2)^2}-\frac{\alpha_q}{2(r^2+d^2)^3}-\frac{6}{r}\ , \tag{2}$$

where $|Y_{lm}\rangle$ are the spherical harmonics, and A_l and ξ_l are l-dependent parameters chosen to fit asymptotic eigenvalues to spectroscopic data [13]. α_d and α_q representing dipole and quadrupole polarizabilities, respectively, were chosen from the review by Dalgarno [14]. The cutoff radius d was determined by Hartree-Fock calculation. These parameters are summarized in Table I. Molecular wave functions were obtained in terms of a linear combination of Slater determinants, and Slater-type orbitals (STO's) are used as basis sets. Fifty-four STO's for O^{5+} and O^{4+} ions and ten STO's for H atoms are used. These Slater exponents used are given in Table II. The precision of the present molecular-state calculation with respect to the spectroscopic data [13] is better than 0.27% for all states. As a measure of the accuracy, the calculated values (Σ states only) for the asymptotic energy are compared with the spectroscopic values in Table III. The calculated asymptotic energies for Π and Δ states are in better agreement with the experimental values than those for the Σ states.

B. Collision dynamics

Expanding the scattering wave function in terms of a product of a molecular state and an atomic-type electron translation factor (ETF) and substituting it into the time-dependent Schrödinger equation, one yields a set of ordinary, linear, first-order coupled equations with the ETF effect in the first order of relative velocity [12]. Under the assumption of straight-line or Coulomb trajectories for heavy-particle motion, the coupled equations can be solved numerically for scattering amplitudes. The square of the scattering amplitude gives a transition probability for the transition $i\rightarrow j$ at a given energy E and impact parameter b. Integration of impact-parameter-weighted probability over impact parameter yields the total cross section. Twenty-two channels are included in the close-coupling calculation: (i) the single-electron-capture $O^{4+}(2snl)$ channel: $nl=4s(\Sigma)$, $4p(\Sigma+\Pi)$, $4d(\Sigma+\Pi+\Delta)$, $4f(\Sigma+\Pi+\Delta)$; (ii) the transfer-excitation $O^{4+}(nln'l')$ channel; $nln'l'=2p3p\ D(\Sigma+\Pi+\Delta)$, $2p3p\ S(\Sigma)$, $2p3p\ P(\Pi)$, $2p3d\ F(\Sigma+\Pi+\Delta)$, $2p3d\ D(\Pi+\Delta)$ $2p3d\ P(\Sigma+\Pi)$; and (iii) the initial $(O^{5+}+H)$ channel from both the triplet and singlet manifolds.

TABLE II. Orbital exponents of the Slater-type orbital basis function.

O^{4+} and O^{5+}			H	
	Exponent			
Orbital	Triplet	Singlet	Orbital	Exponent
2s	13.276 00	13.276 00	1s	2.000 00
	7.479 82	6.132 09 (5.940 51)[a]		1.000 00
	5.977 36	3.651 02 (3.341 05)		0.500 00
	2.964 55	2.875 24 (2.124 87)	2s	0.500 00
2p	4.807 08	4.434 97 (4.440 69)	2p	1.000 00
	2.972 32	2.972 32 (2.958 47)		0.500 00
	2.372 69	1.866 79 (2.010 54)		
3s	1.503 41	1.661 45		
3p	1.648 92	1.719 56 (1.687 95)		
3d	1.682 42	1.627 55		
4s	1.155 38	1.034 92 (1.027 06)		
4p	1.046 24	1.058 43		
4d	1.464 39	1.047 20		
4f	1.239 14	1.210 87		
5s	1.073 45	0.972 10		
5p	1.040 16	0.964 44		
5d	1.002 71	0.908 33		
5f	1.177 36	0.946 79		

[a]AT $R=7.4$–12.5 a.u. we reoptimized some orbital exponents for higher precision and used the value in parentheses.

TABLE III. Calculated and spectroscopic energy levels of the $O^{4+}(1s^2nln'l')$ ion (a.u.).

$nln'l'$	Experiment [13]	Calculation	ΔE (eV)
	Triplet system		
$2p3p(D)$	−6.174 01	−6.170 704	0.0899
$2p3p(S)$	−6.145 39	−6.140 912	0.1218
$2p3p(P)$	−6.120 08	−6.117 063	0.0830
$2p3d(F)$	−6.103 93	−6.097 680	0.1700
$2p3d(D)$	−6.052 99	−6.049 682	0.0900
$2p3d(P)$	−6.034 84	−6.028 559	0.1709
$2s4s(S)$	−5.969 79	−5.955 498	0.3889
$2s4p(P)$	−5.908 45	−5.896 744	0.3185
$2s4d(D)$	−5.879 75	−5.858 755	0.5713
$2s4f(F)$	−5.855 57	−5.839 240	0.4443
	Singlet system		
$2p3p(P)$	−6.196 5	−6.195 610	0.0242
$2p3d(D)$	−6.096 5	−6.085 740	0.2927
$2p3p(D)$	−6.085 0	−6.075 680	0.2535
$2p3p(S)$	−6.037 3	−6.030 800	0.1768
$2p3d(F)$	−6.013 0	−6.000 599	0.3374
$2p3d(P)$	−5.984 3	−5.972 552	0.3196
$2s4s(S)$	−5.927 8	−5.911 800	0.4354
$2s4p(P)$	−5.899 5	−5.887 305	0.3318
$2s4d(D)$	−5.861 2	−5.847 131	0.3828
$2s4f(F)$	−5.845 0	−5.832 086	0.3513
$O^{5+}(2s)+H(1s)$	−5.575 56	−5.562 762	0.3482

III. RESULTS

A. Adiabatic potentials and couplings

Adiabatic potential curves for triplet and singlet manifolds are displayed in Figs 1(a) and 1(b), respectively. For simplicity, only Σ and Π states are shown. Specific locations of avoided crossings and their energy splittings for the triplet and singlet manifolds are given in Table IV as needed for discussions.

1. *Triplet manifold*

For the triplet manifold, the initial channel has a series of avoided crossings with single-electron-capture channels at larger $R \geq 10$ a.u. and with transfer excitation channels at smaller $R < 9$ a.u. The avoided crossings at R_2 and R_5 are expected to play a dominant role in flux promotion, while the avoided crossing at R_4 is important in controlling the branching ratio between single capture and transfer excitation. At R_8 the energy splitting is very small, and the corresponding radial coupling is very sharp (the height and the half-width are about 120 a.u. and 0.01 a.u., respectively). Thus, this crossing is considered to be diabatic and is treated accordingly. (Other avoided crossings that may become important for flux exit at higher energies are those at 5.50 a.u. and 5.62 a.u. among the 7Σ, 8Σ, and 9Σ states, with corresponding energy splittings of 9×10^{-3} and 8×10^{-5} a.u., respectively.) All Π states except for 2Π and 4Π are nearly degenerate with the corresponding Σ states. The 5Π state that correlates with the $O^{4+}(2p3d\ ^3P)$ transfer excitation state lies very close to the single-capture channel $5\Sigma[O^{4+}(2s4s)]$ at $R \leq 9$ a.u. Hence, the 5Σ state is expected to play a crucial role in flux promotion for transfer-excitation process via Π states.

2. *Singlet manifold*

For the singlet manifold, the avoided crossings appear at larger internuclear distance than for the triplet manifold (see Table IV), because the asymptotic energies of the electron capture state are higher than those in the triplet manifold. The cross section of transfer excitation in the singlet manifold is expected to be larger than that in the triplet manifold at lower collision energies, because the energy splitting at R_4 (which connects single capture and transfer excitation) in the singlet manifold is smaller than that in the triplet manifold.

Representative radial couplings for the triplet and singlet manifolds are shown in Figs. 2(a) and 2(b).

B. Transition probabilities

Collision histories as a function of time are displayed for the triplet and singlet manifolds in Figs. 3(a) and 3(b), respectively, at $E=62.5$ eV/amu and $b=6.0$ a.u. Three general observations can be made.

First, the dominant flux transfer takes place among Σ states at avoided crossings. The Π contribution is secondary for most cases at any energy and impact parameter studied. However, the Π contribution is crucial for some states, particularly the triplet $O^{4+}(2s4p)$ state. The contribution of the Δ states is still smaller and perhaps negligible.

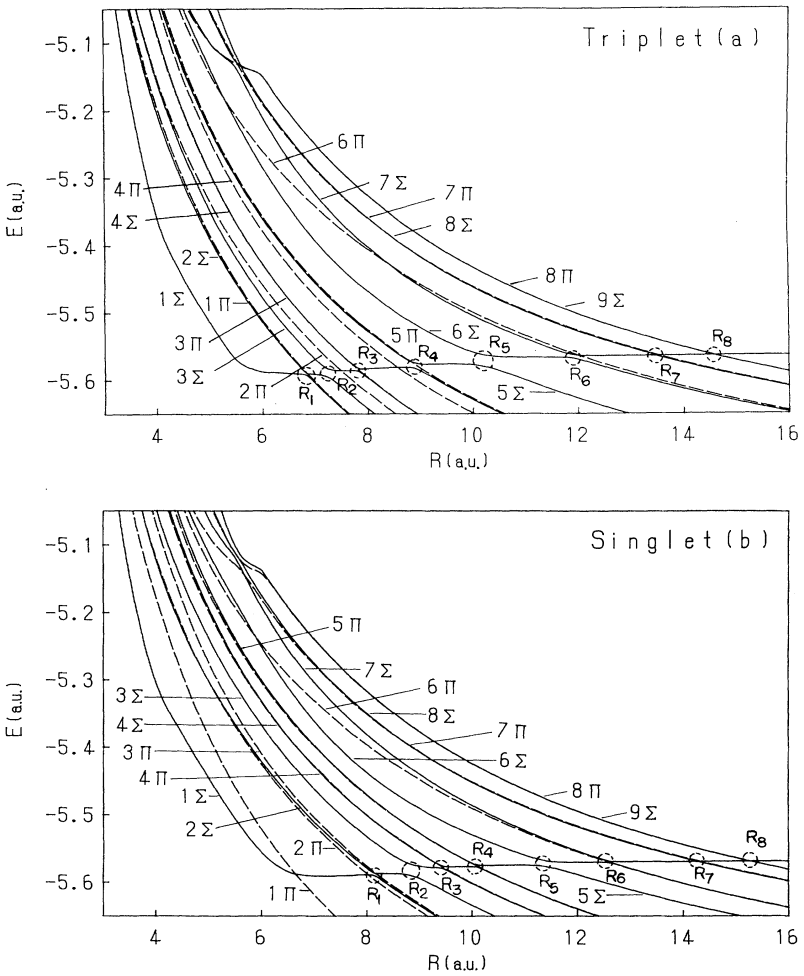

FIG. 1. (a) Adiabatic potential energies for the triplet OH^{5+} manifold. Solid and dashed curves represent Σ and Π states, respectively. 1Σ and 1Π, $O^{4+}(2p3p;^3D)+H^+$; 2Σ, $O^{4+}(2p3p;^3S)+H^+$; 2Π, $O^{4+}(2p3p;^3P)+H^+$; 3Σ and 3Π, $O^{4+}(2p3d;^3F)+H^+$; 4Π, $O^{4+}(2p3d;^3D)+H^+$; 4Σ and 5Π, $O^{4+}(2p3d;^3P)+H^+$; 5Σ, $O^{4+}(2s4s)+H^+$; 6Σ and 6Π, $O^{4+}(2s4p)+H^+$; 7Σ and 7Π, $O^{4+}(2s4d)+H^+$; 8Σ and 8Π, $O^{4+}(2s4f)+H^+$; 9Σ, $O^{5+}(2s)+H(1s)$. Avoided crossings are labeled as R_1, R_2, R_3. . ., and R_8 from smaller R, respectively. (See Table IV.) (b) Adiabatic potential energies for the singlet OH^{5+} manifold. Solid and dashed curves represent Σ and Π states, respectively. 1Π $O^{4+}(2p3p;^1P)+H^+$; 2Π, $O^{4+}(2p3d;^1D)+H^+$; 1Σ and 3Π, $O^{4+}(2p3p;^1D)+H^+$; 2Σ, $O^{4+}(2p3p;^1S)+H^+$; 3Σ and 4Π, $O^{4+}(2p3d;^1F)+H^+$; 4Σ and 5Π, $O^{4+}(2p3d;^1P)+H^+$; 5Σ, $O^{4+}(2s4s)+H^+$; 6Σ and 6Π, $O^{4+}(2s4p)+H^+$; 7Σ and 7Π, $O^{4+}(2s4d)+H^+$; 8Σ and 8Π, $O^{4+}(2s4f)+H^+$; 9Σ, $O^{5+}(2s)+H(1s)$. Avoided crossings are labeled as R_1, R_2, R_3. . ., and R_8 from smaller R, respectively. (See Table IV.)

Second, the initial and first exit $O^{4+}(2s4f)$ states are nearly diabatic in nature (with a unit transition probability), except for very low energies.

Third, as the energy increases, the flux is generally transferred more efficiently to transfer-excitation channels. Their contributions are important even at 6 eV/amu. As the figures clearly show, only the avoided crossings at R_2 and R_5 that connect two transfer excitations and two single captures, respectively, are effective for flux transfer because of their adiabaticity. They actually control the flux exit from one set of channels to another.

C. Cross sections

1. Triplet manifold

Figure 4(a) shows the calculated partial and total cross sections for the triplet manifold. The total cross sections increase slowly, without conspicuous structure, as collision energy decreases. At higher collision energies, above 3 keV/amu, many states contribute equally to the electron capture process. At collision energies from 10 eV/amu to 3 keV/amu, the $O^{4+}(2s4s)$ state is dominant, with the contribution from the $O^{4+}(2s4p)$ state next. Below 100 eV/amu, the transfer-excitation states, $O^{4+}(2p3d;^3P)$ and $O^{4+}(2p3p;^3S)$, contribute up to 15% of the total. As Fig. 1(a) shows, the energy splitting at the avoided crossing R_5 that connects $O^{4+}(2s4s)$ and $O^{4+}(2s4p)$ is large, so the transition is sensitive to the collision energy. Therefore, the flux cannot pass through this point diabatically below 50 eV/amu. Thus, the cross sections of the $O^{4+}(2s4s)$ state decrease, and consequent-

TABLE IV. Locations of avoided crossings and corresponding energy splittings.

	Triplet		Singlet	
Label	Location (a.u.)	Splitting (a.u.)	Location (a.u.)	Splitting (a.u.)
		Transfer excitation		
R_1	6.8	3.0×10^{-3}	8.1	3.5×10^{-3}
R_2	7.2	1.2×10^{-2}	8.8	1.6×10^{-2}
R_3	7.8	5.0×10^{-3}	9.4	3.5×10^{-3}
R_4	8.9	8.0×10^{-3}	10.1	3.5×10^{-3}
		Single electron capture		
R_5	10.2	1.65×10^{-2}	11.5	8.0×10^{-3}
R_6	11.9	5.0×10^{-3}	12.6	2.3×10^{-3}
R_7	13.4	1.0×10^{-3}	14.3	8.0×10^{-4}
R_8	14.6	8.0×10^{-5}	15.3	5.0×10^{-5}

ly those of the $O^{4+}(2s4p)$ state increase. Above 1 keV/amu, the cross sections for the $O^{4+}(2s4d)$ and $O^{4+}(2s4f)$ states increase in what can be interpreted as an increasing role for Π and, to a lesser extent, Δ states to electron capture at this energy domain. Below 0.1 keV/amu, the similar increase in the cross sections for $O^{4+}(2s4d)$ and $O^{4+}(2s4f)$ is due to increasing adiabaticity at the avoided crossings at larger R (R_7 and R_8) and also at smaller R (around 5.5 a.u.). A trajectory effect becomes sizable below 100 eV/amu and translates to the difference of 25% between the straight-line and Coulomb trajectories at $E=62.5$ eV/amu. As we discussed [1,2], the Coulomb trajectory underestimates transitions because of strong repulsion and is not realistic below 100 eV/amu.

2. *Singlet manifold*

The calculated partial and total cross sections for the singlet manifold are shown in Fig. 4(b). Above 0.2 keV/amu, many states contribute equally to electron capture. Compared to the triplet manifold, the contributions of the $O^{4+}(2s4p)$, $O^{4+}(2s4d)$, and $O^{4+}(2s4f)$ states and in particular the $O^{4+}(2p3p\ ^1P,^1D)$ states are large in these energy regions. In the same energy region, the cross section of the $O^{4+}(2s4s)$ state is smaller than that in the triplet manifold. Below 0.2 keV/amu, capture into the $O^{4+}(2s4s)$ and $O^{4+}(2p3p;^1S)$ states becomes equally important. This clear contrast to the triplet manifold occurs because the energy splitting at R_5 of the singlet manifold is smaller than that of the triplet manifold. Because energy splittings at most avoided crossings are small in the singlet manifold, as Fig. 1(b) shows, the flux passes diabatically through all points except R_2 and R_5. At R_2 and R_5, the transition is effectively controlled as sensitive function of collision energy.

3. *Total and partial cross sections and comparison with other results*

Figure 5(a) shows the calculated partial and total cross sections, determined by summing triplet and singlet cross sections with appropriate statistical weights. Because the contribution from the singlet manifold amounts to only 25%, the total cross section is similar to that in the triplet manifold. At higher collision energies, above 2 keV/amu, many states contribute equally to electron capture in an out-of-phase manner, so that the total cross

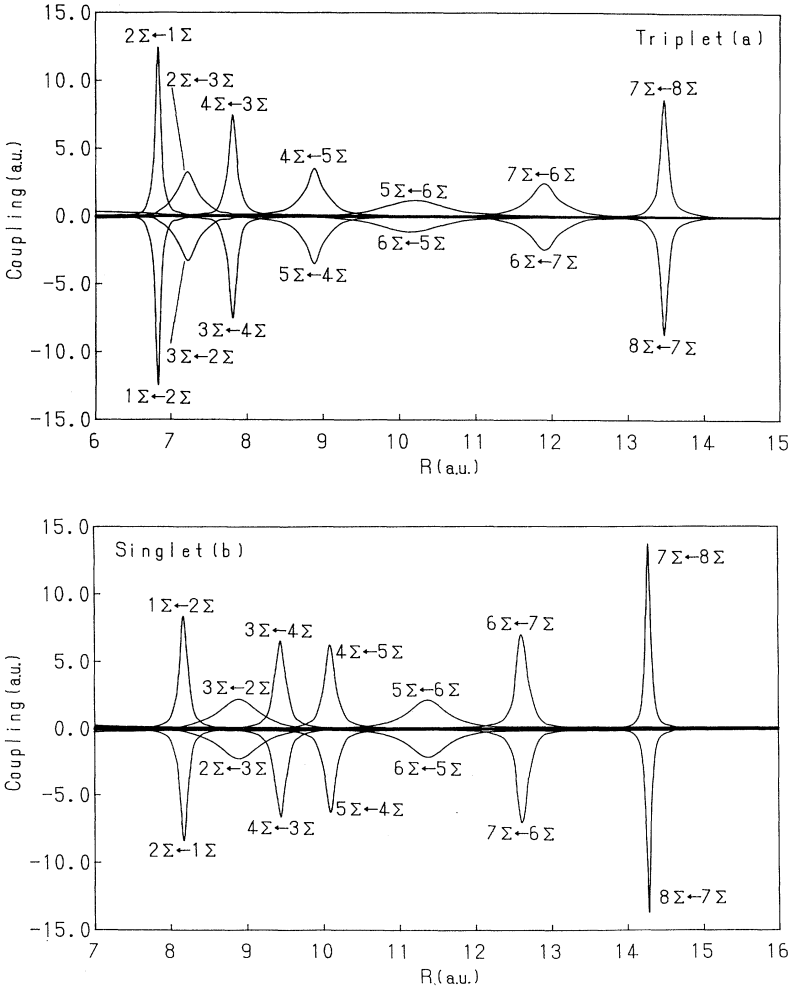

FIG. 2. Representative radial couplings for the (a) triplet and (b) singlet manifolds, respectively.

section appears to be nearly independent of the collision energy. At collision energies lower than 0.7 keV/amu, the $O^{4+}(2s4s)$, $O^{4+}(2s4p)$, and $O^{4+}(2p3p\ ^1S)$ states become the main contributors with an increasing trend and make the cross sections increase slightly. Figure 5(a), also includes the experimental results [5,7]. Our results are in excellent agreement with the measurements over the entire energy region studied.

Figure 5(b) shows only the total and $O^{4+}(2s4l)$ partial cross sections along with results of Andersson, Gargaud, and McCarroll [9]. Although the total cross section of Andersson, Gargaud, and McCarroll is in excellent agreement with our results (and also in good agreement with measurements), their partial cross sections differ significantly from the present results. The discrepancy for $O^{4+}(2s4d)$ is particularly noteworthy. Andersson, Gargaud, and McCarroll included only the one-electron process, neglecting all of the transfer-excitation channels. As our study shows, these transfer-excitation channels make a significant contribution to collision dynamics and are by no means negligible. Neglect of these states is expected to cause overestimation of the cross section for the one-electron process. Therefore, the good agreement of our total cross section and that of Andersson, Gargaud, and McCarroll is considered fortuitous.

D. Transfer-excitation and electron correlation

In this section, we discuss more details of the mechanisms for the transfer-excitation and single-capture processes.

1. Total transfer excitation and single capture

The transfer-excitation and single-electron-capture cross sections for the triplet and singlet manifolds and the

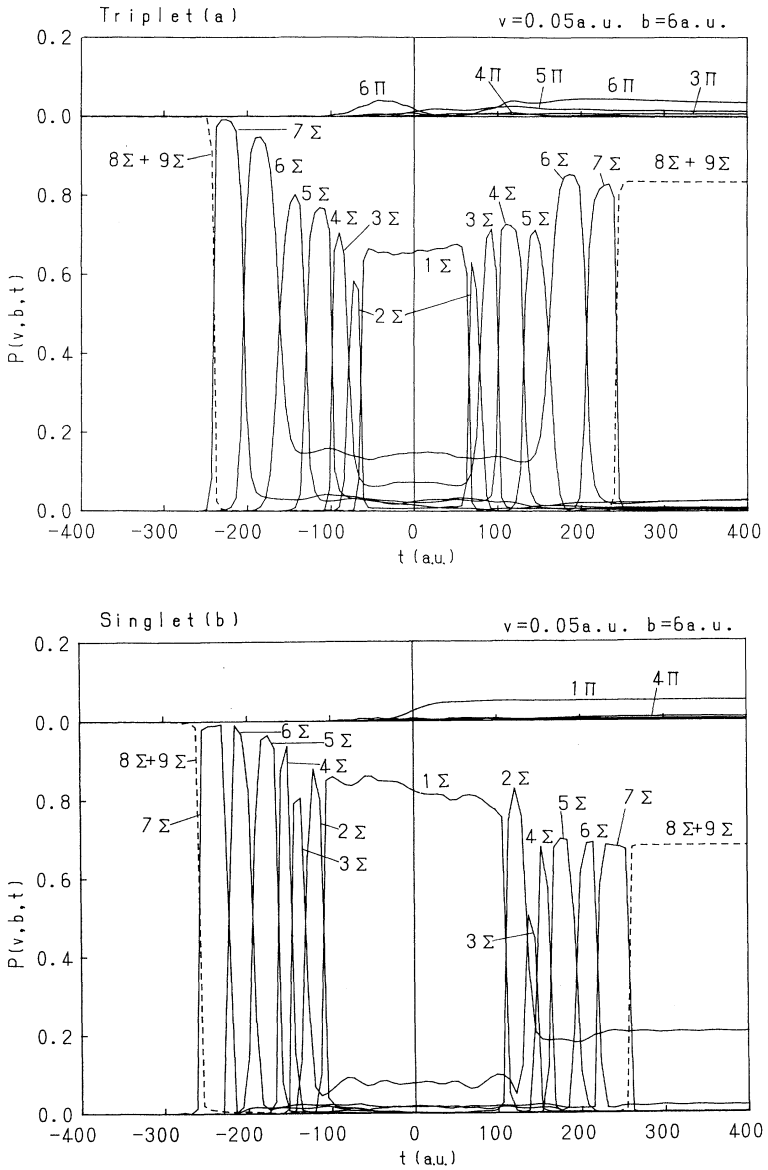

FIG. 3. Collision histories of the transition probabilities as a function of time at $E=62.5$ eV/amu and $b=6.0$ a.u. for a straight-line trajectory for the (a) triplet and (b) singlet manifolds.

totals for each process are presented in Fig. 6. In the triplet manifold, the cross sections of single-electron capture are larger than those of transfer excitation at all collision energies. This tendency becomes more pronounced as the collision energy decreases. In contrast, in the singlet manifold the cross sections of transfer excitation are larger at almost all collision energies than those of single-electron capture, though at lowest and highest collision energies the single-electron-capture process dominates. This finding is interpreted to reflect the energy difference and the coupling strength at avoided crossing R_4, where the energy differences in the triplet and singlet manifolds are 8.0×10^{-3} and 3.5×10^{-3} a.u., respectively. The energy difference in the triplet manifold is larger, and the corresponding coupling is weaker. Hence, at the collision energies considered the transition is less effective at R_4, leaving the flux in single-electron capture channels. In the singlet manifold, the situation is reversed: the energy difference is slightly smaller with stronger coupling, making the transition more effective. Of course, at still lower collision energies in the singlet manifold than those shown in Fig. 6, the flux cannot pass effectively through the avoided crossing R_4, making single-electron capture dominant.

2. *(l,m) distribution*

All of the (l,m) partial cross sections for the triplet and singlet manifolds, respectively, are replotted in Figs. 7(a) through 7(d). The figures indicate that the contributions from the Σ and Π states are similar in magnitude except in some channels [the $O^{4+}(2p3p\ ^3D)$, $O^{4+}(2p3d\ ^3F)$, $O^{4+}(2p3d\ ^1P)$, and $O^{4+}(2s4p\ ^1P)$ states]. The Δ states do not contribute significantly to the electron-capture processes. Generally, the transition to the Π states occurs primarily from Σ states by rotational coupling at regions where Σ and Π states degenerate and from the initial channel through radial coupling at regions of larger b. Thus, if the transition to Π states is to be effective, the Π states must lie close to relevant Σ states and have strong coupling around the turning point or real curve crossing points. In addition, the avoided crossing R_4 is important

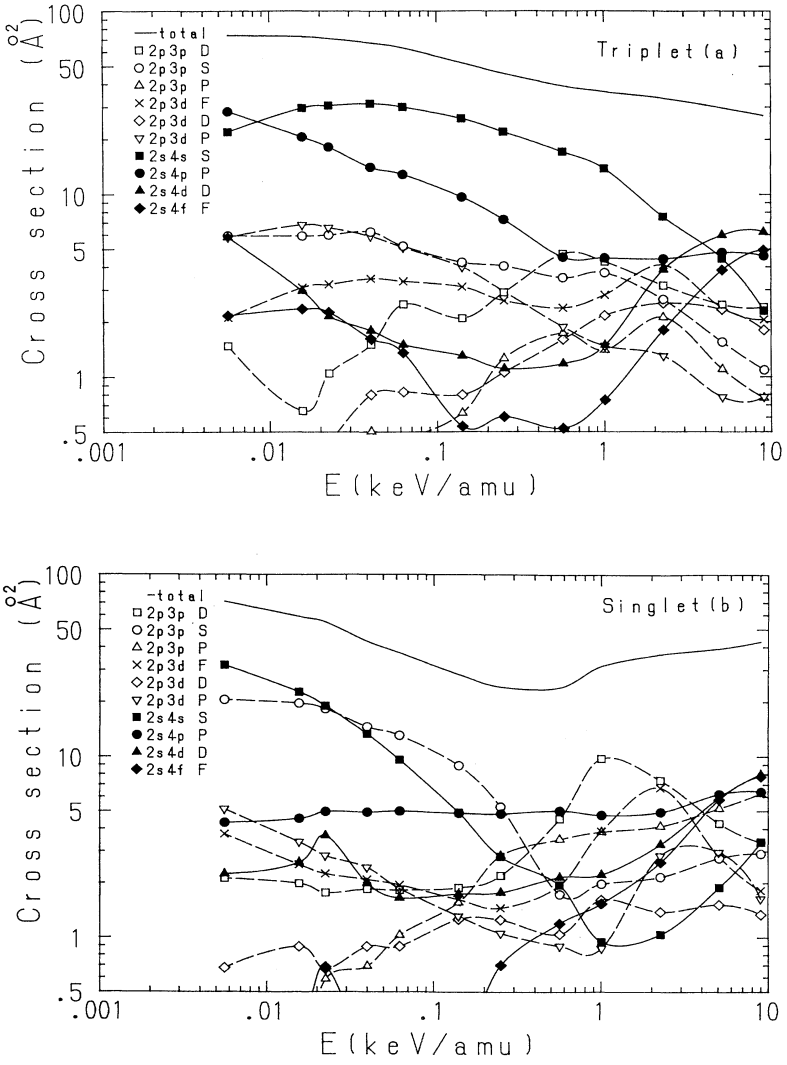

FIG. 4. Total and partial electron capture cross sections for the (a) triplet and (b) singlet manifolds.

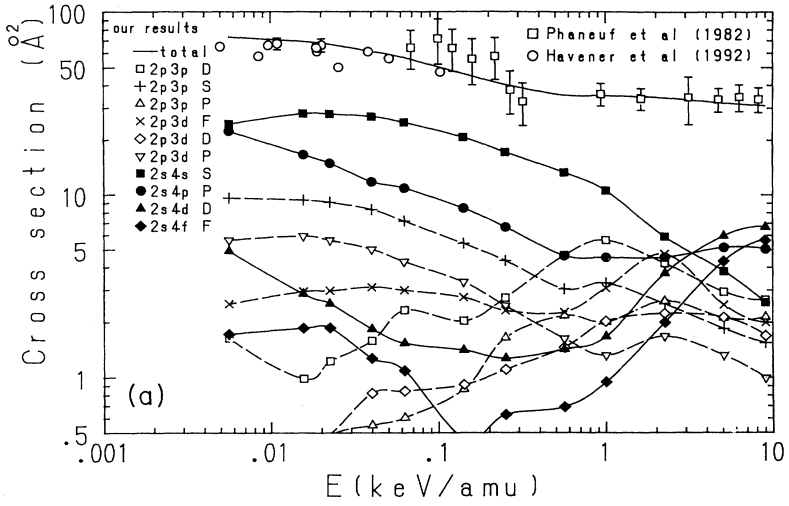

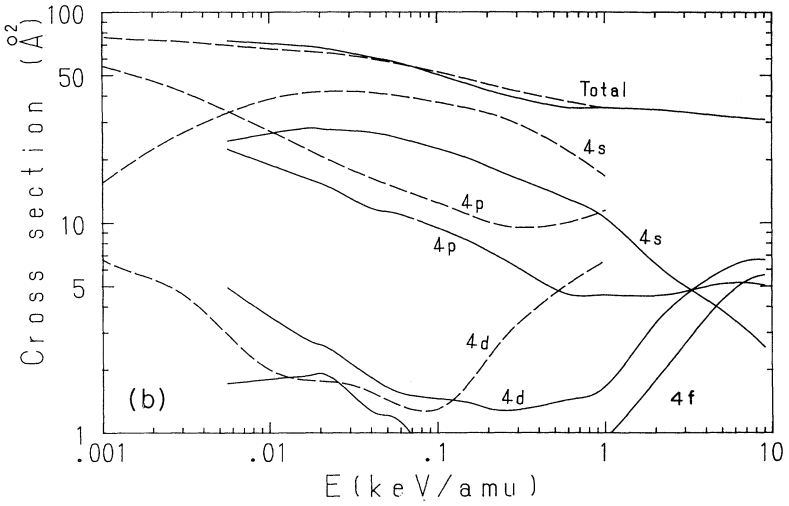

FIG. 5. (a) Statistically weighted total and partial electron capture cross sections. Lines with symbols are from the present work; open symbols are measurements: □, Ref [5]; ○ Ref. [7]. (b) The total and $O^{4+}(2s4l)$ partial cross sections; solid curves are the present results; broken curves are results of Andersson, Gargaud, and McCarroll [9].

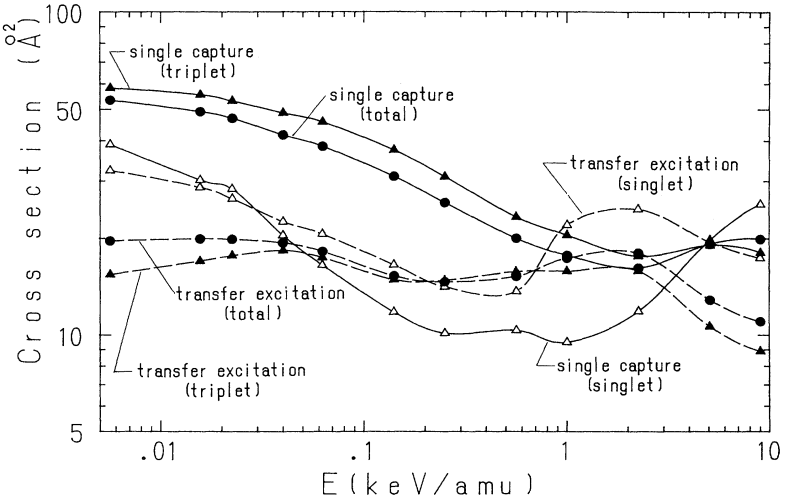

FIG. 6. Cross sections for single-electron capture and transfer excitation. Cross sections of the triplet and singlet manifolds and the statistical weighted sum of these (total) are represented by ▲, △, and ●, respectively. Solid and broken curves represent the results for single-electron-capture and transfer-excitation cross sections, respectively.

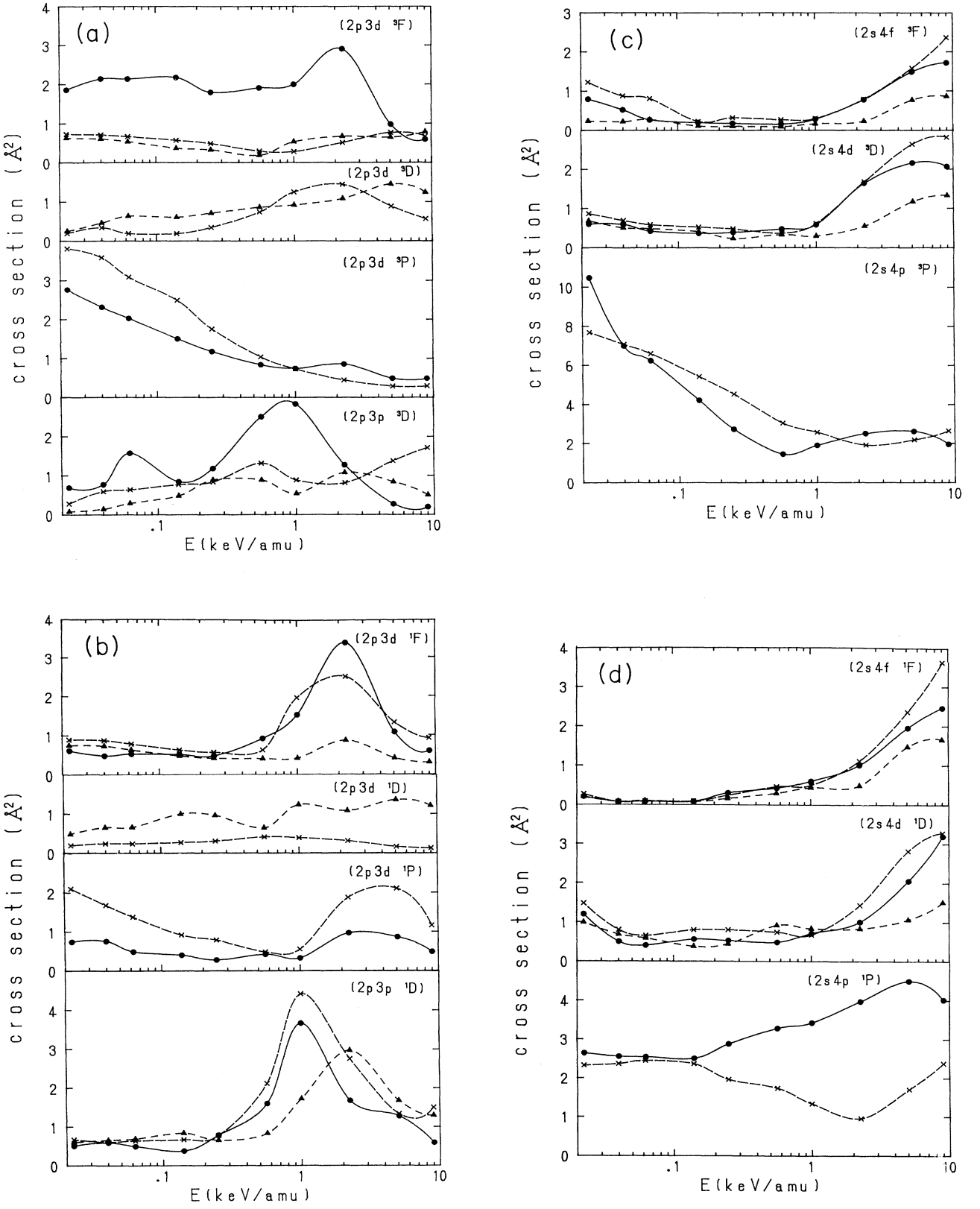

FIG. 7. Partial (l,m) cross sections for transfer excitation and single-electron capture. Solid, broken, and dotted curves represent the cross sections of the Σ, Π, and Δ states, respectively.

in that it separates single-capture and transfer-excitation channels, controlling the branching ratio of the probability. Because the transition mechanism to each channel varies significantly from state to state under a strong correlation of other channels, we examine each case separately.

$O^{4+}(2p3p\ ^{3,1}D)$. The transition to the Σ states proceeds predominantly at the avoided crossing R_1 for both triplet and singlet manifolds. For the Π states, it mainly takes place at small $b<4$ a.u. through a rotational coupling from 3Σ for the triplet. The Π transition in the singlet proceeds at a rather wide range of $b \leq R_1$, resulting in a large transition probability in the intermediate-energy region. The multichannel effect for the transition is far stronger for the triplet, as manifested by the complex pattern of energy dependence in the cross section.

$O^{4+}(2p3d\ ^{3,1}F)$. The transition to the Σ states proceeds mainly at the avoided crossing R_3. That for the Π states takes place in the region of somewhat smaller b through rotational couplings from $4\Sigma(3\Sigma)$ for the triplet (singlet). The energy splitting of the avoided crossing R_3 is twice as large for the triplet and may be in part responsible for larger cross section in the triplet at lower energies.

$O^{4+}(2p3d\ ^{3,1}P)$. The transition to the Σ states proceeds predominantly at avoided crossing R_4, and a larger energy splitting at R_4 in the triplet causes a larger transition probability at lower energies than in the singlet. The Π transition at $R<R_4$ effectively takes place from 5Σ through a rotational coupling. As the flux of the 5Σ in the triplet increases, the transition probability of the Π state also increases.

$O^{4+}(2s4p\ ^{3,1}P)$. Both Σ and Π populate equally for the triplet, while the Σ distribution dominates in the singlet at higher energies. This is because at R_6, where the energy splitting in the triplet is larger than that in the singlet, the cross sections of the triplet become large at lower collision energies. The transitions to Σ states take place at avoided crossing R_6, while the transitions to 6Π have two routes to populate; direct transition from 7Σ and two-step transition from 7Σ through 6Σ. Both routes are sensitive to collision energies, showing a complex pattern for the transition mechanism.

3. *Polarization*

A photon emitted from an excited atom or ion is normally polarized. Its degree of light polarization is defined as

$$P(\theta)=\frac{I_{\parallel}(\theta)-I_{\perp}(\theta)}{I_{\parallel}(\theta)+I_{\perp}(\theta)}\ , \tag{3}$$

where $I_{\parallel}(\theta)$ and $I_{\perp}(\theta)$ are the light intensities with an emitted angle θ parallel and perpendicular to the ion beam direction, respectively. Since the light intensity can be expressed as a function of cross section for a process, the polarization $P(\theta)$ is also a combination of cross-section functions for the process of interest. Here we specifically study single-electron-capture of the $O^{4+}(2s4p)$ level and transfer excitation of the $O^{4+}(2p3d\ F)$ level as examples. For these levels, the polarization (3) for transfer excitation can be explicitly expressed [15] for triplet and singlet manifolds as

$$P^{\rm TE}_{\rm triplet}=\frac{495\sigma_0+495\sigma_1-990\sigma_2}{1537\sigma_0+2909\sigma_1+2414\sigma_2}\ , \tag{4a}$$

$$P^{\rm TE}_{\rm singlet}=\frac{18\sigma_0+18\sigma_1-36\sigma_2}{41\sigma_0+76\sigma_1+58\sigma_2}\ , \tag{4b}$$

and for single-electron-capture as

$$P^{\rm SC}_{\rm triplet}=\frac{15\sigma_0-15\sigma_1}{41\sigma_0+67\sigma_1}\ , \tag{4c}$$

$$P^{\rm SC}_{\rm singlet}=\frac{\sigma_0-\sigma_1}{\sigma_0+\sigma_1}\ , \tag{4d}$$

where σ_0, σ_1 and σ_2 are σ_m cross sections with magnetic quantum number m at given principal and angular quantum numbers (n,l). In the derivation of Eqs. (4a) through (4d), two electrons were explicitly considered. The polarization thus obtained for both levels is shown in Fig. 8 to illustrate the degree of electron correlation (static and dynamic) for the triplet and singlet manifolds as a function of energy.

First, we will discuss polarization of the $O^{4+}(2s4p)$ state. The large disparity in the polarization between the triplet and singlet manifolds is particularly noteworthy. $P^{\rm SC}_{\rm singlet}$ has a peak with the value of 0.85 at 1 keV/amu that is 85% of the theoretical maximum (theoretically, $-1\leq P\leq +1$), implying that the $m=0$ population is dominant. As energy increases, $P^{\rm SC}_{\rm singlet}$ drops rather sharply, to 0.6, and then backs up to 0.75 at 9 keV/amu. In contrast, $P^{\rm SC}_{\rm triplet}$ has either values close to zero or slightly positive values that amount, at most, to 35% of the theoretical maximum value (+0.37) and 4% of the theoretical minimum value (−0.22). Incidentally, this trend in the triplet manifold indicates that transitions in Σ-Σ through a radial coupling or in Σ-Π through a rotational coupling contribute equally to the population, resulting in the small P value.

Next, we will look at the polarization of the

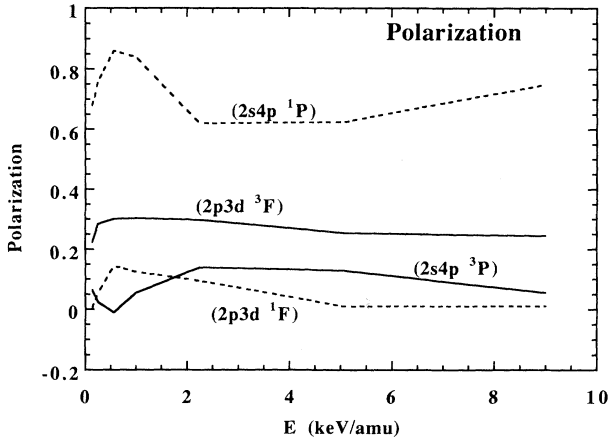

FIG. 8. Polarization for the $O^{4+}(2s4p)$ and $O^{4+}(2p3d\ F)$ states for the triplet and singlet manifolds.

$O^{4+}(2p3d\ F)$ state. The difference in the polarization between the triplet and singlet appears to be smaller than in the previous case, perhaps because when the colliding particles are close enough to induce the transition to this state,the many-channel effect has already mixed the flux well, making many avenues of transition possible and reducing dependence on the spin state. The values of $P^{TE}_{triplet}$ are always positive with, at most, 94% of the theoretical maximum value (+0.32), and they decrease slightly at higher energies. The value of $P^{TE}_{singlet}$ are positive below 5 keV/amu and become nearly null above this energy with only 2% of the theoretical maximum. This trend of having a smaller difference in P values between the triplet and singlet manifolds is common to nearly all transfer-excitation states because of the importance of a close collision that thoroughly mixes the flux. Generally, the difference between the triplet and singlet manifolds arises in part from the difference in dynamic-interaction schemes between electronic spin states and heavy-particle motion.

IV. SUMMARY AND CONCLUSIONS

Electron-capture cross sections have been obtained by applying the semiclassical (22 channels for the triplet and singlet manifolds) molecular-state expansion method with atomic ETF's in the energy range from 6 eV/amu to 10 keV/amu. The calculated results are in excellent agreement with experiments over the entire energy region studied. The Σ and Π states contribute to the capture process, but the contribution of the Δ state is negligible. The contribution from the two-electron process (transfer excitation) is quite large, with 50% in the total cross section at 1 keV/amu. Unless these channels are properly included in the theory, an accurate determination of the cross section will not be possible. Furthermore, the present study reveals a significant difference in collision dynamics and hence in electron correlation between the triplet and singlet manifolds. Experiments that differentiate spin states would be extremely desirable.

ACKNOWLEDGMENTS

This work was supported in part by the U.S. Department of Energy, Office of Energy Research, Office of Health and Environmental Research, under Contract No. W-31-109-ENG-38 (M.K.); by the Office of Basic Energy Science, Division of Chemical Sciences, through Rice University (N.S.); and by the R. A. Welch Foundation (N.S.). N.S. was also supported by a Grant-in-Aid for Scientific Research on Priority Area "Atomic Physics of Multicharged Ions" (Area No. 239/05238204) and "Molecular Magnetism" (Area No. 228/05226215) from the Ministry of Education, Science and Culture of Japan. Some portions of the present calculation were carried out at the computer centers of Tohoku University and Niigata University. The authors are grateful to Dr. Havener for useful comments.

[1] N. Shimakura and M. Kimura, Phys. Rev. A **44**, 1659 (1991).
[2] N. Shimakura, M. Itoh, and M. Kimura, Phys. Rev. A **45**, 267 (1992).
[3] N. Shimakura, S. Koizumi, S. Suzuki, and M. Kimura, Phys. Rev. A **46**, 7876 (1992).
[4] N. Shimakura, S. Suzuki, and M. Kimura, Phys. Rev. A **47**, 3930 (1993).
[5] R. A. Phaneuf, I. Alvarez, F. W. Meyer, and D. H. Crandall, Phys. Rev. A **26**, 1892 (1982).
[6] C. C. Havener, M. S. Huq, H. F. Krause, P. A. Schulz, and R. A. Phaneuf, Phys. Rev. A **39**, 1725 (1989).
[7] C. C. Havener, F. W. Meyer, and R. A. Phaneuf, in *Physics of Electronic and Atomic Collisions,* edited by W. R. Macgillivray, I. E. McCarthy, and M. C. Standage (North-Holland Amsterdam, 1992), p. 381.
[8] M. Gargaud, Ph.D. thesis, Université de Bordeaux I, France ,1987.
[9] L. R. Andersson, M. Gargaud, and R. McCarroll, J. Phys. B **24**, 2073 (1991).
[10] J. Macek and S. Y. Ovchinnikov, Phys. Rev. Lett. **69**, 2357 (1992).
[11] M. Kimura, H. Sato, and R. E. Olson, Phys. Rev. A **28**, 2085 (1983).
[12] M. Kimura and N. F. Lane, in *Advances in Atomic Molecular, and Optical Physics,* edited by D. R. Bates and B. Bederson (Academic, New York, 1989), Vol. 26, p. 79.
[13] S. Bashkin and J. R. Stoner, Jr., *Atomic Energy Levels and Grotrian Diagrams I* (North-Holland, Amsterdam, 1975).
[14] A. Dalgarno, Adv. Phys. **11**, 281 (1962).
[15] R. Hoekstra, Ph.D thesis, University of Groningen, Netherlands, 1990.